Materials Science & Engineering C 107 (2020) 110264

Contents lists available at ScienceDirect

Materials Science & Engineering C

journal homepage: www.elsevier.com/locate/msec

Comparison of 2D and 3D cell culture models for cell growth, gene expression and drug resistance

Julia C. Fontoura[a,b], Christian Viezzer[a], Fabiana G. dos Santos[c], Rosane A. Ligabue[c], Ricardo Weinlich[d], Renato D. Puga[d], Dyeison Antonow[e], Patricia Severino[d], Cristina Bonorino[b,f,*]

[a] Laboratório de Imunologia Celular e Molecular, Pontifícia Universidade Católica do Rio Grande do Sul (PUCRS), Porto Alegre, RS, Brazil
[b] Departamento de Ciências Básicas da Saúde, Universidade Federal de Ciências da Saúde, Porto Alegre, RS, Brazil
[c] Laboratório de Caracterização de Materiais, PUCRS, Porto Alegre, RS, Brazil
[d] Hospital Israelita Albert Einstein, São Paulo, SP, Brazil
[e] Institute of Petroleum and Natural Resources (IPR), Tecnopuc, PUCRS, Porto Alegre, RS, Brazil
[f] Department of Surgery, School of Medicine, University of California at San Diego, United States

A B S T R A C T

In vitro drug screening is widely used in the development of new drugs, because they constitute a cost-effective approach to select compounds with more potential for therapy. They are also an attractive alternative to *in vivo* testing. However, most of these assays are done in two-dimensional culture models, where cells are grown on a polystyrene or glass flat surface. In order to develop *in vitro* models that would more closely resemble physiological conditions, three-dimensional models have been developed. Here, we introduce two novel fully synthetic scaffolds produced using the polymer polyhydroxybutyrate (PHB): a Solvent-Casting Particle-Leaching (SCPL) membrane; and an electrospun membrane, to be used for 3D cultures of B16 F10 murine melanoma cells and 4T1 murine breast cancer cells. A 2D cell culture system in regular tissue culture plates and a classical 3D model where cells are grown on a commercially available gel derived from Engelbreth-Holm Swarm (EHS) tumor were used for comparison with the synthetic scaffolds. Cells were also collected from *in vivo* tumors grown as grafts in syngeneic mice. Morphology, cell viability, response to chemotherapy and gene expression analysis were used to compare all systems. In the electrospun membrane model, cells were grown on nanometer-scale fibers and in the SCPL membrane, which provides a foam-like structure for cell growth, pore sizes varied. Cells grown on all 3D models were able to form aggregates and spheroids, allowing for increased cell-cell contact when compared with the 2D system. Cell morphology was also more similar between 3D systems and cells collected from the *in vivo* tumors. Cells grown in 3D models showed an increase in resistance to dacarbazine, and cisplatin. Gene expression analysis also revealed similarities among all 3D platforms. The similarities between the two synthetic systems to the classic EHS gel model highlight their potential application as cost effective substitutes in drug screening, in which fully synthetic models could represent a step towards higher reproducibility. We conclude PHB synthetic membranes offer a valuable alternative for 3D cultures.

1. Introduction

Cancer is estimated to have caused over 9.6 million deaths in 2018, still being considered one of the major causes of death worldwide [1]. Tumor types and tumor infiltrating cells are highly heterogeneous, adding to the complexity of the disease. Thus, development of new treatments is a constant, crucial and challenging struggle. One logistic problem in these efforts is that most drug screenings are performed in two-dimensional (2D) *in vitro* cultures, which disregard the complexity of interactions seen in tumors *in vivo*. When in 2D, cells have more surface area in contact with the plastic and culture media than with other cells [2] forcing them into a polarization that does not reflect physiological conditions. A more realistic model of *in vitro* cancer cell cultures is the use of three-dimensional (3D) cultures. They are generally either scaffold-based models, in which cells interact with a substrate, or scaffold-free models, in which cells are unable to attach to a surface, thus forcing cell aggregation and spheroid formation.

In scaffold-based 3D cultures, cells are grown on a substrate that mimics the extracellular matrix (ECM). They are usually further classified into hydrogels or solid scaffolds, and may be either of natural or synthetic origin (Reviewed in: [3]; [4]). One of the most widely accepted 3D cultures is a hydrogel made from the extract of Engelbreth-Holm Swarm (EHS) tumors, being commercially available as Matrigel® (Corning), Geltrex® (Invitrogen) and Cultrex® (Trevigen). EHS tumors produce a high amount of basement membrane proteins, the most abundant being laminin, collagen IV, entactin, fibronectin, and heparin sulfate proteoglycan; also, these extracts contain a great number of growth factors [5,6]. Culturing cells on an EHS gel may not only alter morphology and gene expression patterns [7], but also migration [8], cell cycle and proliferation [9]. Nevertheless, because this basement

* Corresponding author. Departamento de Ciências Básicas da Saúde, Universidade Federal de Ciências da Saúde, Porto Alegre, RS, Brazil.
E-mail addresses: cristinabcb@ufcspa.edu.br, cbonorino@ucsd.edu (C. Bonorino).

https://doi.org/10.1016/j.msec.2019.110264
Received 16 February 2019; Received in revised form 12 September 2019; Accepted 28 September 2019
Available online 14 October 2019
0928-4931/

membrane gel support is obtained from a murine tumor, attention should be given when culturing non-murine cells on such model. Dijkstra et al. observed $CD4^+$ T cells reactivity when they were in contact with the gel or with dendritic cells exposed to Geltrex® [10]. There is also a great concern when using EHS gels regarding batch to batch variations [6,11]. These variations may significantly alter experiments, as the Matrigel® Growth Factor Reduced was shown to have only 53% similarity between batches [6].

Another technique for scaffold-based approaches is producing membranes through electrospinning. This technique produces fiber matts with adjustable diameter and porosity, while having a large surface area and an interconnected pore structure [12]. These scaffolds may be obtained from different types of materials, mostly natural or synthetic polymers, though also ceramics and metals may be used. As such, scaffolds have been used in different fields, being in tissue engineering [13], water filtration, drug development as a delivery system [14,15], and *in vitro* 3D cell culture [16].

Besides electrospinning, another commonly used technique is Solvent-Casting Particle-Leaching (SCPL), which can produce foam-like membranes. It was developed in 1994 [17], and has been used in a number of studies since then, especially on bone tissue engineering [18,19], though also in vascular repair [20]. SCPL is an approach much simpler than electrospinning, as the polymer solution is mixed with a porogen (usually salt) and left to dry, followed by leaching in order to remove the porogen used, being relatively easy to adjust pore size.

Among the different materials used for scaffold fabrication, polyhydroxybutyrate (PHB) is a very promising one. It is a natural polymer from the polyhydroxyalkanoate family and was first discovered in bacteria. In these organisms, PHB is stored as long chains and used as a source of energy, though it has already been found in various organisms. Because of PHB's highly flexible structure, biocompatibility and biodegradability [21], it has been used in many different areas, be it as bio-implanted patches [22], drug delivery carriers [23], wound dressing [24], scaffolds for cell growth for tissue engineering [25,26] and as a 3D cell culture model [27].

The aim of this work was to construct and characterize two novel synthetic scaffolds for 3D cultures for tumor models. We test here two different scaffold producing techniques, electrospinning and SCPL, using the same polymer, PHB. The scaffold topography is compared with EHS gel cell culture, one of the most commonly used 3D models. Cell morphology, gene expression and response to drug treatment were also assessed and compared between the three systems, as well as 2D conventional cultures. Our results indicate that the two synthetic systems developed by us are similar to the classic EHS gel model, highlighting their potential application as cost effective substitutes for drug screening.

2. Materials and methods

2.1. Membrane production

2.1.1. Electrospinning

PHB (Sigma Aldrich) was solubilized in chloroform at 60 °C for 45 min, treated with dimethylformamide (20% v/v) for 30 min at room temperature and bathed in a steady ultrasound pulse of 40 kHz for 20 min. A glass syringe with the polymer solution was attached to an infusion bomb and to its needle was applied an electric current of +14 kV and −1 kV. The polymer was collected on a static collector, and membranes were kept in a vacuum chamber for chloroform evaporation for 48 h, after which they were kept frozen at −20 °C.

2.1.2. Solvent-Casting Particle-Leaching (SCPL)

After solubilizing the polymer as described above, the solution was poured in a casting mold. Then, sieved salt particles below 53 μm were added and the chloroform was left to evaporate for 72 h in an exhaustion hood. The membrane was then kept in deionized water for an ultrasonic bath of 40 kHz for 1 h, washed and then kept in an ultrasonic bath for another hour. It was then placed for 72 h in a vacuum chamber to dry, followed by storage at −20 °C.

2.2. Scaffold characterization

Solid EHS gel 10 mg/ml was fixed with Karnovski solution, followed by a gradual dehydration with acetone and critical point dried. EHS gel, electrospun and SCPL membranes were mounted on stubs and sputter-coated with gold for Field Emission Gun Scanning Electron Microscopy (FESEM, Inspect 50 FEI) analysis. Pore and fiber diameters were measured using the ImageJ software by using the set scale and measurement functions, for each group was considered a minimum of 4 images and on average 20 measurements per image.

2.3. Membrane preparation and cell seeding

Before each experiment, the electrospun and SCPL membranes were sterilized by washing three times in ethanol 70%, followed by three washes in phosphate buffer saline (PBS), being at least 10 min for each wash. The membranes were then placed on a 96-well culture plate at 37 °C and 5% CO_2 for up to 24 h. For the EHS gel cultures, Geltrex® LDEV free (Invitrogen) at a concentration of 10 mg/ml was added to the wells and left to solidify at 37 °C, 5% CO_2 for 1 h. The medium used for the culture was supplemented with 2% of EHS gel. The gel solution was manipulated in ice to avoid premature gelling.

Mouse melanoma B16F10 GFP cells (kindly provided by Dr. Martim Bonamino from the Brazilian National Cancer Institute, INCA) and mouse breast cancer 4T1 cells (ATCC CRL-2539) were grown in DMEM High glucose (Gibco) and RPMI-1640, respectively, both supplemented with 10% Fetal Bovine Serum (FBS). Cultures were kept in a humidified atmosphere of 5% CO_2 and 37 °C until use. Each of these models had a different cell growth surface, which may alter proliferation rates. We thus performed pilot experiments, in order to determine the most adequate number of cells to be inoculated in each model, so that we could comparatively analyze, in the same amount of culture time, growth both in presence or absence of chemotherapy drugs. Thus, for the experiments, cells at 80% confluence in 2D cultures were detached with trypsin solution and seeded at 10^2 cells/well for 2D cultures; $2{,}5*10^4$ cells/well for EHS gel; 10^4 and $2{,}5*10^4$ cells/well for B16F10 GFP and 4T1 cells on electrospun membranes; and $2{,}5*10^4$ cells/well for SCPL cultures. For the electrospun and SCPL groups, cells were seeded on top of each membrane in 30 μl and left to adhere at 37 °C and 5% CO_2 for 1 h, after which the medium was completed to 200 μl. After 24 h, the membranes were carefully washed with PBS and changed to another well. Cultures were kept for 7 days and medium was changed twice.

2.4. In vivo tumor model

C57BL/6 and BALB/c mice between 6 and 8 weeks old and 15–20 g were obtained and housed at the Centro de Modelos Biológicos e Experimentais (CEMBE PUC-RS, Brazil), where they had food and water *ad libitum*. C57BL/6 animals were inoculated subcutaneously with 10^6 B16F10 GFP cells on the left flank, while BALB/c were inoculated with 10^5 4T1 cells in the third left mammary fat pad. After 10 and 17 days for B16F10 GFP and 4T1 cells, respectively, the animals were euthanized and tumors were harvested. Both tumors were cut and kept in a Karnovski solution for FESEM analysis (section 2.5), while half of the B16F10 GFP tumor was minced for RNA extraction (section 2.8). All animal procedures used were approved by PUC-RS university's animal ethic committee (CEUA), having the protocol ID CEUA 8466.

2.5. Scanning electron microscopy

After 7 days of culture, samples were fixed with a Karnovski

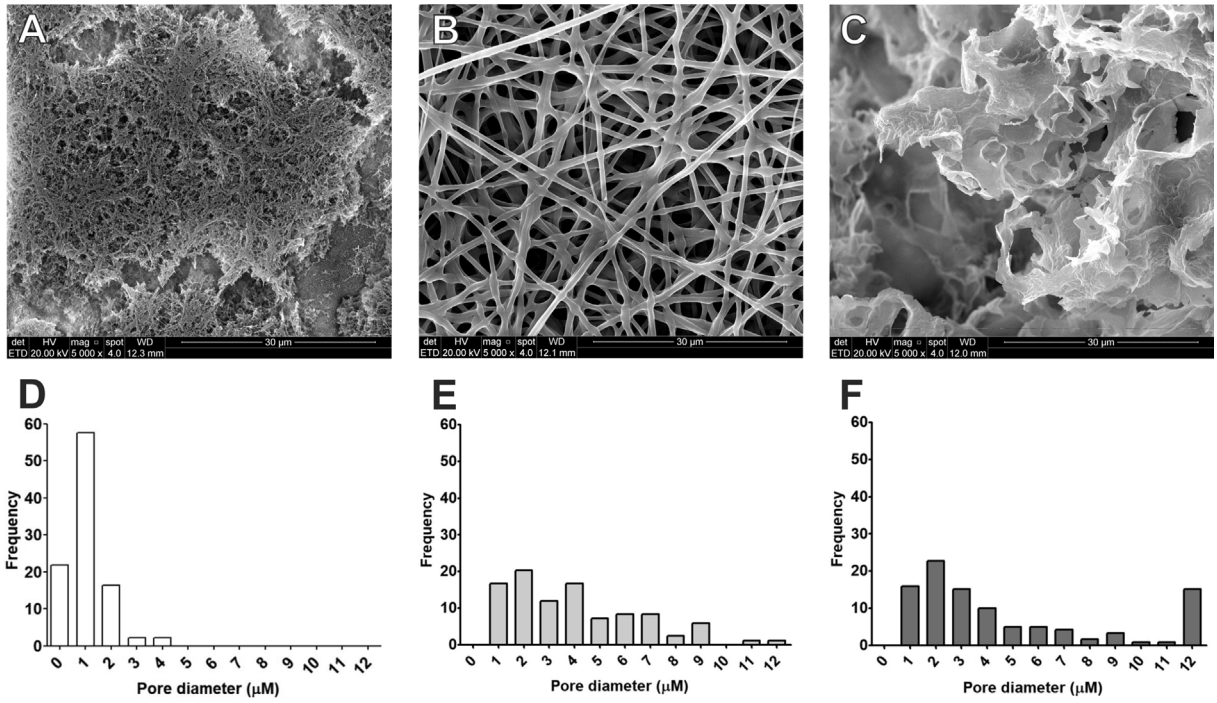

Fig. 1. Scaffold structures. FESEM micrographs of the different scaffolds studied, **(A)** EHS gel, **(B)** electrospun, **(C)** SCPL membrane. Magnification of 5,000x, scale bar 30 μM. Pore diameter of the different scaffolds, **(D)** EHS gel, **(E)** electrospun, **(F)** SCPL membrane.

solution, followed by post-fixation with osmium tetroxide for 1 h, and a slow and gradual dehydration with acetone. Samples were critical point dried, mounted in stubs and sputter-coated with gold. Visualizations were done through FESEM (Inspect 50 FEI).

2.6. Confocal microscopy

B16F10 GFP samples were fixed with 4% paraformaldehyde, quenched with NH_4Cl 50 mM for 5 min, permeabilized with 0,2% PBS-Triton for 5 min and blocked with 1% PBS-bovine serum albumin (BSA) for 30 min. B16F10 GFP cells were then incubated with Hoechst for 5 min, followed by 3 washes with PBS, 5 min each. Samples were kept on PBS-Glycerol (1:1) until imaging on a confocal laser scanning microscope (Zeiss LSM 710), images were analyzed by Photoshop.

2.7. Cell viability (MTT)

After 5 days in culture, cells were treated with either cisplatin (100 and 200 μM) or dacarbazine (1000 and 2000 μM), doses chosen from dose-dependent curves done on 2D cultures (data not shown). At the end of the 48 h incubation, 20 μl of MTT solution (5 mg/ml) was added to each well, including blank samples composed of the respective model with medium and no cells. The plate was then kept on an incubator at 37 °C and 5% CO_2. After 3 h the plate was centrifuged at 1500 RPM, 4 °C, and medium was discarded carefully while on ice. Formazan crystals were dissolved with 200 μl of DMSO and the plate was kept lightly shaking for 10 min, followed by optical density reading on Anthos Zenyth 340r microplate reader between 570 and 620 nm. Readings were normalized to their respective control without drug treatment and data analyzed on GraphPad prism 5.

2.8. Microarray

RNA was extracted from samples using the PureLink® RNA Mini Kit (Thermo Fisher). Briefly, cells were washed with ice-cold PBS, lysis buffer was added directly to cells and the protocol was carried out according to the manufacturer's instructions. RNA integrity was assessed using the Agilent 2100 Bioanalyzer and the RNA 6000 Nano Kit (Agilent Technologies, Santa Clara, CA, USA) and total RNA was stored at −80 °C until use. Gene expression was analyzed using DNA microarrays SurePrint G3 8 × 60K (Agilent, USA). Cyanine-3 labeled RNA from samples and cyanine-5 labeled reference RNA (Universal Reference RNA, Agilent Technologies) were combined and hybridized to microarrays following manufacturer's protocols (LowInput QuickAmp Labeling Kit Two-Color, Agilent, USA). Microarrays were scanned using the SureScan (Agilent, USA), according to default parameters, and experiment quality, background correction, and the identification of expressed genes were carried out with the Feature Extraction software v12 (Agilent, USA). From the data set, probes were mapped to the reference *Mus musculus* genome (mm9, available at http://hgdownload.cse.ucsc.edu/downloads.html#mouse) using the software package Burrows-Wheeler Aligner (BWA). Based on this alignment, a total of 4598 probes were used in this work (Table S1, Supporting information). Data analysis was carried out using GeneSpring software v12.6 (Agilent). We used quantile normalization for fluorescence intensity normalization between samples, and only probes identified as detected or not detected in at least 100% of one of the experimental conditions were selected for the identification of differentially expressed genes (ANOVA, cut-off for significance p-value < 0.05). Gene expression levels are presented in fold-changes in respect to cells cultivated in monolayer (2D). The overall structure of the dataset was visualized with the unsupervised method principal components analysis (PCA) (GeneSpring, Agilent). Hierarchical clustering of differential gene expression is presented in the form of heat maps using Euclidean distance and Ward's or complete linkage (GeneSpring, Agilent, and Morpheus software) and a Venn diagram was used to illustrate differences and similarities between the datasets [28]. Gene Ontology (GO) term and KEGG pathways enrichment analysis were carried out using DAVID Bioinformatics Resources 6.8 and results were considered statistically significant if p-value < 0.05 after Benjamini-Hochberg False-Discovery Rate (FDR) correction [29].

Table 1
Pore size in μM across 3D models.

	Min	Max	Mean	Median
EHS gel	0.21	4.35	1.06 ± 0.76	0.89
Electrospun	0.66	12.07	4.04 ± 2.66	3.55
SCPL	0.56	48.36	6.66 ± 9.22	3.04

3. Results and discussion

3.1. Scaffold production and characterization

Through electrospinning and SCPL techniques two types of membranes were generated and their topography can be seen on Fig. 1A–C. While gel fibers had small diameters, with a mean of 0.043 ± 0.02 μm (Fig. S1A, Supporting information), electrospun fibers had larger diameters, with a mean of 1.1 ± 0.47 μm (Fig. S1B, Supporting information). Since SCPL membranes had a different production approach from electrospun membranes, it was only possible to measure its pore diameter, as they are not composed of fibers. Instead, these SCPL membranes were composed of random shapes, with pore sizes varying between 0.56 and 48.36 μm, while electrospun membrane pores and gel pores varied between 0.66-12.07 μm and 0.21–4.35 μm, respectively (Fig. 1D–F, Table 1). Pore size is a very important and discussed issue regarding scaffold models since it can determine how the cells will interact and grow. It has been proposed that in order for cells to grow on a "true 3D" environment, pore sizes should be smaller than the cells. This way, cells may interact more closely with the scaffold. Small pore diameters can also prevent cells from growing alongside fibers, which may be no different than a 2D curved plane [30]. Besides, depending on cell type, nanopatterns have been shown to either promote or inhibit cell attachment [31], or even affect differentiation of myoblasts [32]. It is agreed, though, that the pore diameter should be related to the size of the cells being cultured. As has been seen by Lowery et al., human dermal fibroblasts grew better on scaffolds with pore sizes between 6 and 20 μm. Larger pores would promote growth along fibers and decrease ECM production, and though smaller ones allowed cells to bridge fibers and produce ECM much faster, they would only grow on top of the membrane [33]. For that, varying pore sizes may promote cell penetration into the scaffold, where it may grow interacting more closely with this ECM mimetic [34].

3.2. Cell culture morphology

As has been seen before, cells cultured *in vitro* may alter their morphology according to the conditions in which they are grown in. Triple-negative breast cancer cells (MDA-MB-231) after being cultured on 15% PCL electrospun scaffolds showed a higher elongation factor than cells grown on 2D cultures [16]. Besides, different breast and prostate cancer cell lines showed distinct cell organizations when growing on a 3D environment, as compared with 2D cultures, allowing better drug investigation [7,35]. In order to evaluate cell growth across different culture methods, we employed two approaches: Field Emission Gun Scanning Electron Microscopy (FESEM) and confocal microscopy analysis. Both were performed after culturing cells for either 7 days *in vitro* or 10 days for B16F10 GFP melanoma cells on C57BL/6 and 14 days for 4T1 breast cancer cells on Balb/c mice. As can be seen by FESEM on Fig. 2 for B16F10 GFP, while there are few cell aggregates on 2D cultures, cells grown on 3D environments were organized in slightly larger aggregates (Fig. 2A). Melanoma cells on 3D cultures sometimes showed a rounder morphology, viewed by FESEM in the larger magnification detail (Fig. 2A), more closely resembling *in vivo* than 2D growth. Interestingly, cells on EHS gel, electrospun membrane and SCPL membrane showed a variety of morphologies, similarly to B16F10 GFP cells on C57BL/6 mice. Morphological differences can also be observed by confocal microscopy (Fig. 2B), where round and elongated cells are seen in more detail. While all cells are elongated in 2D cultures, 3D systems showed both round and elongated cells in the aggregates. Though melanoma cells on both SCPL and electrospun membranes were able to infiltrate the scaffolds, those on the SCPL membrane tended to grow involving the scaffold structure instead of forming spheroids on top of the substrate, as seen on electrospun samples (Fig. 2C). Additionally, cell aggregates on the electrospun membrane had more spherical cells than the other 3D models, and they were also formed on a much higher frequency than on the SCPL membrane (Fig. 2C). B16F10 growing on the 3D models also had a number of filopodia, traditionally interpreted as interaction with a 3D structure.

As expected, B16F10 GFP cells and 4T1 cells showed different growth characteristics. While B16F10 cultured on EHS gel usually grows spheroids that will merge and form large irregular spheroids, 4T1 tended to have smaller, better-defined round spheroids, which even if merged together, would retain its round conformation. Besides, B16F10 GFP cells when grown on 3D models form cell aggregates and have a rounder morphology than what is seen on 2D, however, the same cannot be said about 4T1 cells. These breast cancer cells, when grown on membranes, seem to mostly maintain their elongated morphology (Fig. 3A). Still, although 4T1 cells don't appear to readily form cell aggregates, they can easily be seen infiltrating the electrospun membrane, which might allow them to interact more, providing an environment similar to spheroids. Especially on the SCPL membrane, cells were able to grow and envelop the scaffold (Fig. 3B). Still, each model has its own structure and characteristics, leading to different cell-cell and cell-ECM interactions. Besides, different cell lines may also react differently to the same stimuli.

It has already been reported that cells grown on a tissue culture plastic tend to have a more flattened morphology. Human breast cancer cells (MCF7), after growing on 2D were flat with trigonal and polygonal morphologies, while cells grown on a collagen scaffold had a diversity of morphologies, including rounder, spread-out and elongated [36]. Besides, endometrial cell lines when cultured in EHS gels formed glandular and spheroid-like structures, resembling much more closely *in vivo* morphology [37]. In general, the formation of cell aggregates or spheroids has been shown to better simulate tissues, especially when considering that not all cells will get in contact with medium or drugs due to difficulties in nutrient and waste exchange. Depending on the spheroid size, it may be composed of cells on three different stages: cells on the outermost layer will proliferate, while those in the middle layer will be quiescent; and if the structure is large enough (usually diameter above 500 μm), it will have a necrotic core due to nutrient inaccessibility and increased acidity and waste products [38]. Thus, the formation of these cell aggregates and spheroids on the 3D cultures studied may bring advantages to the models by providing different microenvironments for the cells. Although spheroids less round in shape may have a different structure than the classical ones (since it may develop more than one necrotic center), it may still provide different microenvironments in cell culture, hence altering response to signals.

3.3. Effect of chemotherapeutics on 2D and 3D models

In order to evaluate how the two novel models proposed here, SCPL and electrospun membranes, would affect cell response to chemotherapy, cultures were treated for 48 h with either cisplatin (CDDP) or dacarbazine (DTIC) followed by MTT cell viability analysis. As can be seen on Fig. 4, cells grown on EHS gel showed increased resistance in all drug concentrations used. Such response is expected, as there have been various reports regarding this phenomena [39,40]. Similar to EHS gel cultures, cells on membranes were able to better withstand DTIC treatment than control, however, they only showed a tendency towards CDDP resistance.

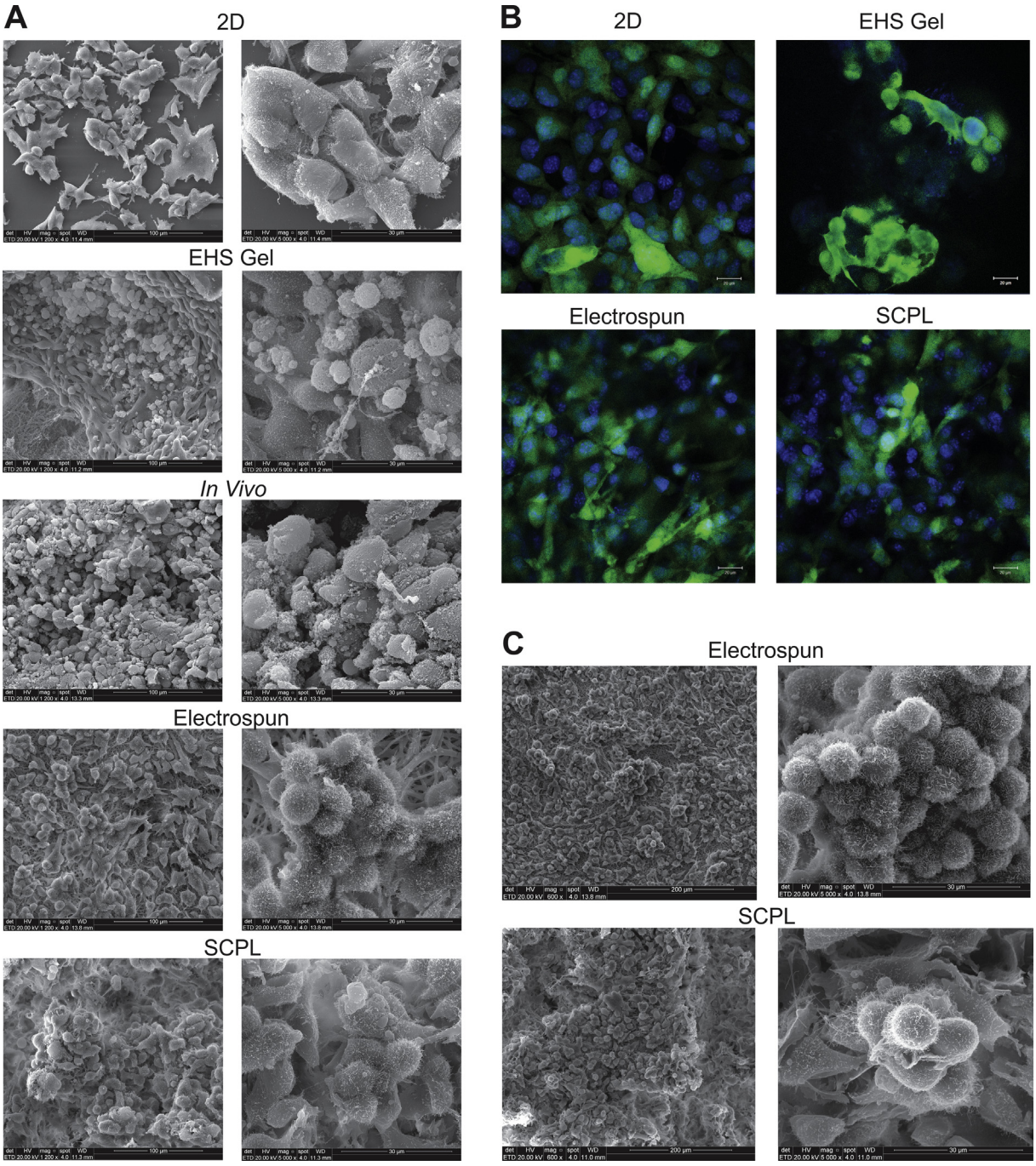

Fig. 2. Morphological differences in B16F10 GFP cell cultures grown in different scaffolds (A) FESEM micrographs comparing culture *In vitro* for 7 days and *In vivo* 10 days tumor of B16F10 GFP cells on C57BL/6 mice. Left panel, 1200x; right panel, detail of the upper panel with magnification 5000x. **(B)** Confocal images showing growth *in vitro* after 7 days in culture, where nuclei are stained in blue, and in green GFP produced by the melanoma cells. **(C)** FESEM micrographs of B16F10 GFP growth structures on electrospun and SCPL membranes after 7 days in culture. Left panel, magnification 600x; Right panel, detail with magnification 5000x. (For interpretation of the references to colour in this figure legend, the reader is referred to the Web version of this article.)

Cells cultured on 3D models may display either increased or decreased drug resistance when compared with results from 2D cell cultures. In prostate cancer cell lines, it was found that compounds targeting the mTOR pathway inhibited cancer cells in 2D and 3D cultures, while those targeting the AKT pathway were less effective on 2D [35]. It has also been shown that spheroids on collagen gel showed greater resistance to doxorubicin treatment than cells on 2D and spheroids on a scaffold-free model [41]. These results come to show that depending on the 3D environment and cell-cell and cell-matrix interactions, a culture might become resistant or susceptible to a certain drug treatment. In fact, a number of ways through which resistance can be affected has been described. One was studied by Imamura et al., where dense spheroids had a tendency to be resistant to paclitaxel and doxorubicin treatment when compared to looser spheroids or 2D growth. These denser spheroids showed decreased apoptosis and stained positive for Ki67, while having hypoxic centers [42]. Colorectal cancer cell lines have also been shown to have decreased p53 levels on 3D cultures after CDDP treatment, when compared with 2D treated cultures. Even though these cells would have similar p53 levels on 2D and 3D, after CDDP treatment cells cultured in 3D had decreased sensitivity to the

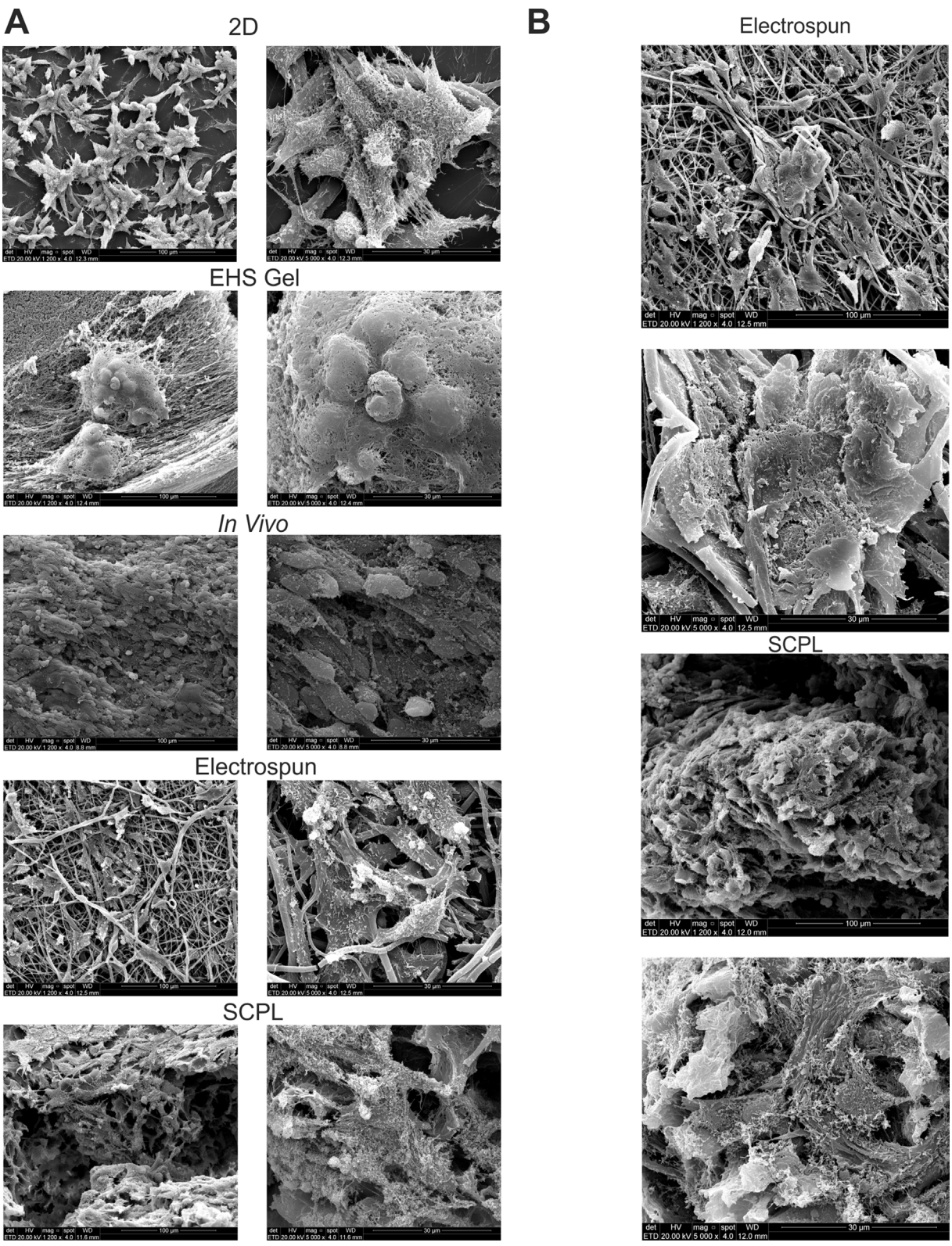

Figure 3. 4T1 breast cancer cell culture in different cell culture systems. FESEM micrographs of **(A)** comparison of cell culture on different models, where cells *in vitro* were grown for 7 days and *In vivo* on Balb/c mice for 14 days. **(B)** Cells grown on electrospun and SCPL scaffolds for 7 days, showing spheroid formation and thorough membrane embracing, respectively.

drug. These alterations were attributed to the difference in architecture between 2D and 3D cultures [43]. It is believed that cell morphology and interactions between cells may have a great effect on expression and treatment outcome. As seen on MCF7 breast cancer cells, treatment with CDDP on EHS gel had chromatin reorganization leading to induction of ATR phosphorylation, chk1 activation and REV3L upregulation, leading to increased senescence [39].

Interestingly, both CDDP and DTIC mainly act by crosslinking with

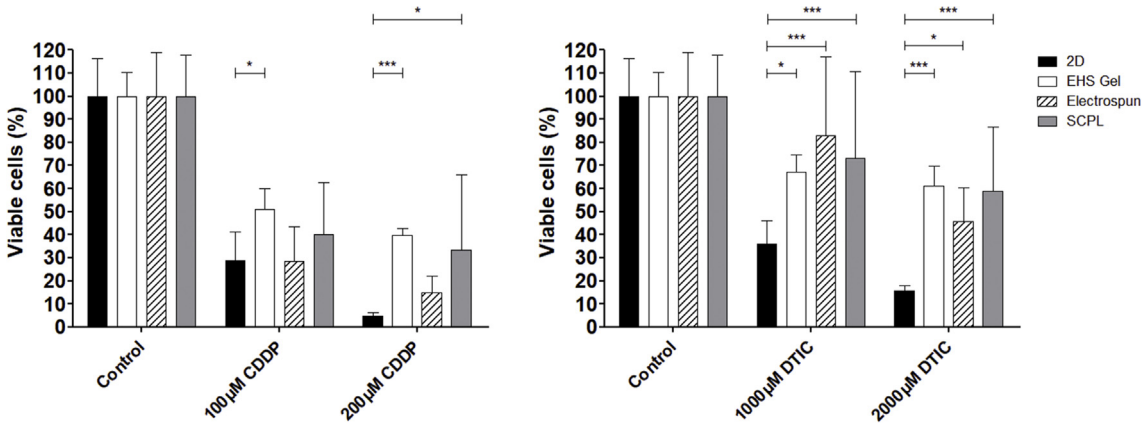

Fig. 4. Viability analysis through MTT. B16F10 GFP cells were cultured for 7 days, followed by treatment with either Cisplatin, CDDP (100 or 200 µM) or Dacarbazine, DTIC (1000 or 2000 µM) for 48 h * for $p < 0.05$ and *** for $p < 0.001$.

DNA (with a platinum or alkyl group, respectively) [44], and both had at least a tendency for drug resistance, not seen on 2D cultures. These differences are probably due to distinct pathways being activated after treatment. Still, all 3D cultures were able to provide an environment with a scaffold to which cells were able to adhere. Cells treated with cisplatin and cultured on SCPL membrane might have had in general a higher resistance due to increased penetration and interaction of cells with the scaffold, when compared with culture on electrospun membranes.

3.4. RNA expression across different culture models

We compared global gene expression profiles of exponentially growing B16F10 GFP cells in monolayer (2D) with the 3D culture conditions (ElMb, SCPL and EHS gel) and cells collected *in vivo*. The PCA plot indicates that the majority of the variability in the dataset is associated with cell source (2D, 3D or *in vivo*): samples from each culture model grouped together (Fig. 5A).

The tree view representing the variation in gene expression highlights that cells cultivated *in vivo* showed the most significant differences when compared with the 2D cell culture, followed by EHS gel (Fig. 5B, for a complete list of differentially expressed transcripts, considering a fold-change of 2, see Table S2**,** Supporting information). Gene ontology (GO) term and KEGG pathways gene enrichment analysis were carried out to understand if these changes in gene expression levels were related to biological processes involved in the differences in 3D cultures, such as tissue development and cell adhesion, or in response to radio- and chemotherapy, such as cell proliferation, cell death and DNA repair systems. No such differences were found. However, cells collected *in vivo*, EHS gel, and SCPL showed similar alterations in transcription-related processes (RNA synthesis) when compared with cells cultivated in monolayer, as highlighted by the enrichment of GO term Transcription, DNA Template (GO:0006351) (Table S3, Supporting information). For the electrospun membrane, this enrichment was not as evident (p-value above the significance level), but a group of genes associated with this process was also deregulated (Table S3, Supporting information). A summary of the overlap between the 3D cultivation systems can be visualized in the Venn diagram (Fig. 5C) and specific characteristics of each dataset are available as supporting information (Table S4).

When the *in vivo* samples were analyzed, differences in the up regulation of genes from immune system processes were noteworthy (LGALS3, HCK, UNC93B1, TFEB, TLR3, SERPING1, LGALS9, BTK, PSMB9, ZAP70, C1RL, NRROS, BCL6, PRDM1, C2, CD79A) as well as in cytoskeleton organization (DLC1, FMNL1, CORO1A, DOCK2, PRR5, TMSB4X, BCL6, IQSEC*3, CAPZB, FLNA, IQSEC2)*.

The expression level of gene transcripts previously associated with cancer in the 3D systems was analyzed in more detail, because these models were developed for studies in cancer progression and drug response. We selected genes grouped within KEGG database under the term “Pathways in Cancer” and evaluated the overall gene expression in each system, including genes involved in processes as diverse as cell-cell contact, cell migration, cell death and cell proliferation (a complete scheme for these pathways is available at https://www.genome.jp/kegg-bin/show_pathway?mmu05200). Table 2 lists the genes of the KEGG pathways that showed differential expression between each culture system and cells collected *in vivo* when compared with cells cultivated in monolayer. From a total of 534 genes, 52 were differentially regulated between the 3D systems and the monolayer culture, or among themselves. A comprehensive view of the variation between each system is depicted in Fig. 5D.

RNA expression is commonly found altered after modifying cell culture conditions or with tumor development. Lymphoid enhancer binding factor 1 (LEF1), which is associated with the Wnt pathway, had increased expression in all 3D and *in vivo* models when compared with the 2D cell culture. This result is expected, as malignant melanoma patients have been shown to have increased LEF1 when compared with peritumoral tissue and benign nevus [45]. Patients with malignant melanoma have also shown increased serum levels of the Vascular Endothelial Growth Factor (VEGF) in comparison to healthy controls [46]. These results have also been obtained *in vitro*, when T47D breast cancer cells were grown as spheroids and showed increased VEGFA expression [47]. This aspect has also been recapitulated in our experiments, where all 3D cell cultures and *in vivo* model have shown increased expression of VEGFA when compared to 2D cell cultures. As with other genes mentioned, our 3D cultures have been able to approximate to *in vivo* models, exemplifying another way through which they might be better suited for *in vitro* cell culture than the 2D cell culture model.

4. Conclusions

All the culture methods analyzed were able to sustain cell growth, and all 3D cell culture models showed morphologies more similar to *in vivo* growth than to the monolayer cell culture. Both electrospun and SCPL membranes did not induce cell death, and cells grown on them were able to interact with each other and with the ECM mimetic, which was true for both melanoma B16F10 and breast cancer 4T1 cells. After drug treatment with dacarbazine, cells grown in all 3D culture systems showed increased resistance compared to those grown in monolayer, showing at least 30% more viability than the 2D group. After cisplatin treatment, cells grown on both electrospun and SCPL membranes displayed a tendency for increased drug resistance - though only cells grown on EHS gel had statistically significant increased viability.

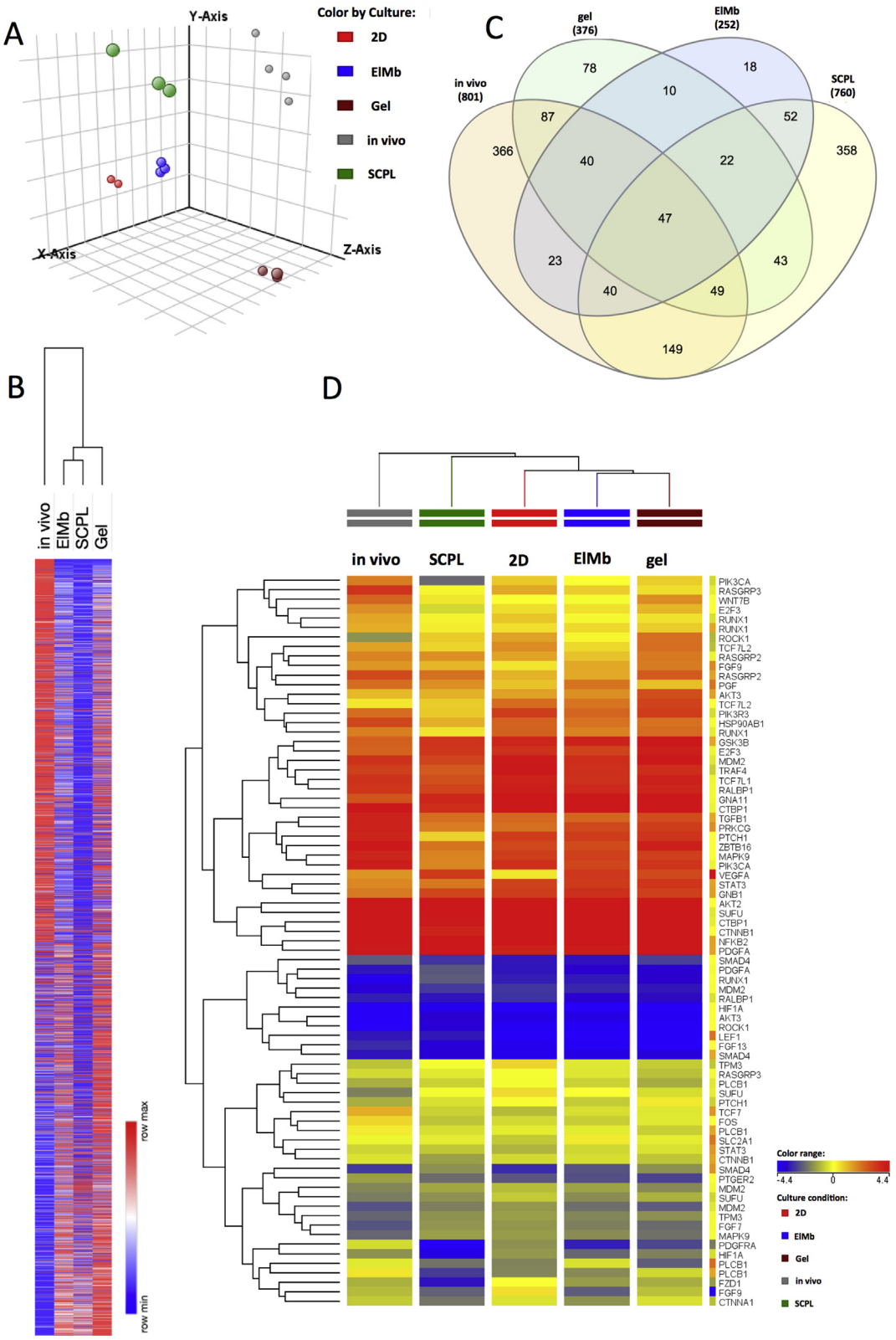

Fig. 5. Microarray analysis comparing gene expression across the different cell culture methods. **(A)** Principal component analysis (PCA) of the source of variation in the gene expression dataset. This is an exploratory statistical method that simplifies the microarray data. Shown here is the average signal of each sample in a three-dimensional space of the first three principal components. Each culture condition clusters separately. (**B**) Hierarchical clustering of gene expression changes between each cultivation system and the monolayer (2D) cell culture. Differentially expressed genes are plotted according to their degree of respective co-expression. Values are represented in log2Foldchange. The cultivation system is indicated at the top, columns represent samples, while rows represent genes. The degree of correlation between genes or samples is plotted in a tree view fashion. (**C**) Venn diagram. Summary the overlap between differentially expressed genes in each dataset. (**D**) Hierarchical clustering of genes belonging to Pathways in Cancer (KEGG Pathways). Values from each culture system are represented in as normalized intensity and include only genes that showed at least a 2-fold change difference when compared with the monolayer culture. 2D: monolayer cell culture; ElMb: electrospun membrane; Gel: EHS gel; SCPL: Solvent-Casting Particle-Leaching membrane.

Table 2
Differentially expressed genes belonging to KEGG Pathways in Cancer (mmu0520) between 3D cell culture systems and cells collected *in vivo* compared with cells cultivated in monolayer. Only genes showing at least a 2-fold change are listed.

KEGG PATHWAY – Pathways in Cancer: mmu0520		
Cell Source	Gene Symbol -Up regulated	Gene Symbol -Down regulated
In vivo	TCF7, PTGER2, PGF, LEF1, FGF13, PRKCG, ZBTB16, TGFB1, FOS, WNT7B, RASGRP3, RASGRP2, VEGFA, PDGFRA, PLCB1	E2F3, FGF7, ROCK1, FGF9, GNA11, FZD1, TCF7L2, SUFU, STAT3, TPM3, GNB1, GSK3B, TRAF4, AKT2
EHS gel	WNT7B, PDGFA, VEGFA, RASGRP2, SMAD4, LEF1, ZBTB16, NFKB2, PLCB1, AKT3	FGF9, PDGFRA, FZD1, SUFU, TPM3
Electrospun membrane	PGF, VEGFA, SLC2A1, LEF1	ROCK1, FGF9, PDGFRA, FZD1, CTNNA1, TCF7L2, TPM3
SCPL	RASGRP2, SMAD4, LEF1, VEGFA	HSP90AB1, CTBP1, FGF9, RALBP1, GNA11, FZD1, CTNNA1, TCF7L2, TCF7L1, CTNNB1, HIF1A, RASGRP3, PDGFRA, PIK3CA, MDM2, MAPK9, PTCH1, PIK3R3, PLCB1, RUNX1, TRAF4, AKT2

Gene expression analysis corroborated the similarities between 3D and *in vivo* groups in relation to 2D, that were observed in the previous biological assays, having relatively few transcripts showing different expression between the models. Even though these 3D models were produced by different techniques, they showed many similarities across experiments, demonstrating that the use of animal origin models such as the EHS gel could be substituted by fully synthetic 3D scaffolds. Further experiments using different conditions such as RNA collection time point and cell stimulation, may identify other differences in molecular mechanisms associated with cell growth and maintenance in each studied model.

Acknowledgements

Special thanks to MSc. Karina Lima, PhD. Rodrigo Gassen and PhD. Sofia Scomazzon from Pontifícia Universidade Católica do Rio Grande do Sul (PUCRS) for support, as well as Leandro Baum and colleagues from Central Laboratory of Microscopy and Microanalysis (LabCEMM) at PUCRS for the FESEM technical support, and to Thiago P. A. Aloia from Hospital Israelita Albert Einstein for the Confocal Microscopy technical support. This work was supported by the Programa Nacional de Apoio à Atenção Oncológica (PRONON) SIPAR 250000.159946/2014-16. J. C. Fontoura was the recipient of a scholarship from Coordenação de Aperfeiçoamento de Pessoal de Nível Superior (CAPES) and Cristina Bonorino of a fellowship from Conselho Nacional de Desenvolvimento Científico e Tecnológico (CNPq).

Appendix A. Supplementary data

Supplementary data to this article can be found online at https://doi.org/10.1016/j.msec.2019.110264.

References

[1] F. Bray, J. Ferlay, I. Soerjomataram, R.L. Siegel, L.A. Torre, A. Jemal, Global cancer statistics 2018: GLOBOCAN estimates of incidence and mortality worldwide for 36 cancers in 185 countries, CA Cancer J. Clin. 68 (2018) 394–424, https://doi.org/10.3322/caac.21492.

[2] B.M. Baker, C.S. Chen, Deconstructing the third dimension – how 3D culture microenvironments alter cellular cues, J. Cell Sci. 125 (2012) 3015–3024, https://doi.org/10.1242/jcs.079509.

[3] S. Sanyal, Culture and Assay Systems Used for 3D Cell Culture, Corning, 2014.

[4] M.W. Tibbitt, K.S. Anseth, Hydrogel as extracellular matrix mimics for 3D cell culture, Biotechnol. Bioeng. 103 (2010) 655–663, https://doi.org/10.1002/bit.22361.Hydrogels.

[5] R.D. Simoni, J.B. Hays, T. Nakazawa, S. Roseman, R. Stein, O. Schrecker, H.F. Lauppe, H. Hengstenberg, J. Thompson, H. Towbin, T. Staehelin, J. Gordon, E.B. Waygood, R.L. Mattoo, N. Weigel, M.A. Kukuruzinska, A. Nakazawa, E.G. Waygood, W. Wray, T. Boulikas, V.P. Wray, R., B. Hancock, Basement membrane complexes with biological activity, Proc. Natl. Acad. Sci. U.S.A. 25 (1986) 312–318, https://doi.org/10.1021/bi00350a005.

[6] C.S. Hughes, L.M. Postovit, G.A. Lajoie, Matrigel: a complex protein mixture required for optimal growth of cell culture, Proteomics 10 (2010) 1886–1890, https://doi.org/10.1002/pmic.200900758.

[7] P.A. Kenny, G.Y. Lee, C.A. Myers, R.M. Neve, J.R. Semeiks, P.T. Spellman, K. Lorenz, E.H. Lee, M.H. Barcellos-Hoff, O.W. Petersen, J.W. Gray, M.J. Bissell, The morphologies of breast cancer cell lines in three-dimensional assays correlate with their profiles of gene expression, Mol. Oncol. 1 (2007) 84–96, https://doi.org/10.1016/j.molonc.2007.02.004.

[8] R. Poincloux, O. Collin, F. Lizárraga, M. Romao, M. Debray, M. Piel, P. Chavrier, Contractility of the cell rear drives invasion of breast tumor cells in 3D Matrigel, Proc. Natl. Acad. Sci. 108 (2011) 1943–1948, https://doi.org/10.1073/pnas.1010396108.

[9] M. Gargotti, U. Lopez-Gonzalez, H.J. Byrne, A. Casey, Comparative studies of cellular viability levels on 2D and 3D *in vitro* culture matrices, Cytotechnology 70 (2018) 261–273, https://doi.org/10.1007/s10616-017-0139-7.

[10] K.K. Dijkstra, C.M. Cattaneo, F. Weeber, M. Chalabi, J. van de Haar, L.F. Fanchi, M. Slagter, D.L. van der Velden, S. Kaing, S. Kelderman, N. van Rooij, M.E. van Leerdam, A. Depla, E.F. Smit, K.J. Hartemink, R. de Groot, M.C. Wolkers, N. Sachs, P. Snaebjornsson, K. Monkhorst, J. Haanen, H. Clevers, T.N. Schumacher, E.E. Voest, Generation of tumor-reactive T cells by Co-culture of peripheral blood lymphocytes and tumor organoids, Cell 174 (2018) 1586–1598, https://doi.org/10.1016/j.cell.2018.07.009 e12.

[11] G. Benton, I. Arnaoutova, J. George, H.K. Kleinman, J. Koblinski, Matrigel: from discovery and ECM mimicry to assays and models for cancer research, Adv. Drug Deliv. Rev. 79–80 (2014) 3–18, https://doi.org/10.1016/j.addr.2014.06.005.

[12] L. Jesús Villarreal-Gómez, M. Cornejo-Bravo, R. Vera-Graziano, D. Grande, Electrospinning as a powerful technique for biomedical applications: a critically selected survey, J. Biomater. Sci. 27 (2016) 157–176, https://doi.org/10.1080/09205063.2015.1116885.

[13] J. Ramier, D. Grande, T. Bouderlique, O. Stoilova, N. Manolova, I. Rashkov, V. Langlois, P. Albanese, E. Renard, From design of bio-based biocomposite electrospun scaffolds to osteogenic differentiation of human mesenchymal stromal cells, J. Mater. Sci. Mater. Med. 25 (2014) 1563–1575, https://doi.org/10.1007/s10856-014-5174-8.

[14] E. Yan, Y. Fan, Z. Sun, J. Gao, X. Hao, S. Pei, C. Wang, L. Sun, D. Zhang, Biocompatible core-shell electrospun nanofibers as potential application for chemotherapy against ovary cancer, Mater. Sci. Eng. C 41 (2014) 217–223, https://doi.org/10.1016/j.msec.2014.04.053.

[15] S. Chen, S. Kumar Boda, S.K. Batra, X. Li, J. Xie, Emerging roles of electrospun nanofibers in cancer research, Adv. Healthc. Mater. 7 (2017), https://doi.org/10.1002/adhm.201701024.

[16] M. Rabionet, M. Yeste, T. Puig, J. Ciurana, Electrospinning PCL scaffolds manufacture for three-dimensional breast cancer cell culture, Polymers (Basel) 9 (2017) 1–15, https://doi.org/10.3390/polym9080328.

[17] A.G. Mikos, A.J. Thorsen, L.A. Czerwonka, Y. Bao, R. Langer, Preparation and characterization o poly(L-lactic acid) foams, Polymer (Guildf). 35 (1994) 1068–1077, https://doi.org/10.1002/anie.196904562.

[18] Z.L. Mou, L.M. Duan, X.N. Qi, Z.Q. Zhang, Preparation of silk fibroin/collagen/hydroxyapatite composite scaffold by particulate leaching method, Mater. Lett. 105 (2013) 189–191, https://doi.org/10.1016/j.matlet.2013.03.130.

[19] N. Thadavirul, P. Pavasant, P. Supaphol, Fabrication and evaluation of polycaprolactone–poly(hydroxybutyrate) or poly(3-hydroxybutyrate-co-3-hydroxyvalerate) dual-leached porous scaffolds for bone tissue engineering applications, Macromol. Mater. Eng. 302 (2017) 1–17, https://doi.org/10.1002/mame.201600289.

[20] L. Rogers, S.S. Said, K. Mequanint, The effects of fabrication strategies on 3D scaffold morphology, porosity, and vascular smooth muscle cell response, J. Biomater. Tissue Eng. 3 (2013) 300–311, https://doi.org/10.1166/jbt.2013.1088.

[21] R.N. Reusch, Physiological importance of poly-(R)-3-hydroxybutyrates, Chem. Biodivers. 9 (2012) 2343–2366, https://doi.org/10.1002/cbdv.201200278.

[22] E.C.C. Reis, A.P.B. Borges, C.C. Fonseca, M.M.M. Martinez, R.B. Eleotério, G.O. Morato, P.M. Oliveira, Biocompatibility, osteointegration, osteoconduction, and biodegradation of a hydroxyapatite-polyhydroxybutyrate composite, Braz. Arch. Biol. Technol. 53 (2010) 817–826, https://doi.org/10.1590/S1516-89132010000400010.

[23] X. Wang, S.S. Liow, Q. Wu, C. Li, C. Owh, Z. Li, X.J. Loh, Y.L. Wu, Codelivery for paclitaxel and bcl-2 conversion gene by PHB-PDMAEMA amphiphilic cationic copolymer for effective drug resistant cancer therapy, Macromol. Biosci. 17 (2017) 1–11, https://doi.org/10.1002/mabi.201700186.

[24] E.I. Shishatskaya, E.D. Nikolaeva, O.N. Vinogradova, T.G. Volova, Experimental wound dressings of degradable PHA for skin defect repair, J. Mater. Sci. Mater. Med. 27 (2016) 165, https://doi.org/10.1007/s10856-016-5776-4.

[25] C. Ye, P. Hu, M.-X. Ma, Y. Xiang, R.-G. Liu, X.-W. Shang, PHB/PHBHHx scaffolds

and human adipose-derived stem cells for cartilage tissue engineering, Biomaterials 30 (2009) 4401–4406, https://doi.org/10.1016/j.biomaterials.2009.05.001.
[26] Z. Karahaliloğlu, M. Demirbilek, M. Şam, N. Sağlam, A.K. Mizrak, E.B. Denkbaş, Surface-modified bacterial nanofibrillar PHB scaffolds for bladder tissue repair, Artif. Cells Nanomed. Biotechnol. 44 (2016) 74–82, https://doi.org/10.3109/21691401.2014.913053.
[27] Y. Wang, X.L. Jiang, S.W. Peng, X.Y. Guo, G.G. Shang, J.C. Chen, Q. Wu, G.Q. Chen, Induced apoptosis of osteoblasts proliferating on polyhydroxyalkanoates, Biomaterials 34 (2013) 3737–3746, https://doi.org/10.1016/j.biomaterials.2013.01.088.
[28] H. Heberle, V.G. Meirelles, F.R. da Silva, G.P. Telles, R. Minghim, InteractiVenn: a web-based tool for the analysis of sets through Venn diagrams, BMC Bioinf. 16 (2015) 169, https://doi.org/10.1186/s12859-015-0611-3.
[29] Y. Benjamini, Discovering the false discovery rate, J. R. Stat. Ser. Soc. B Stat. Methodol. 72 (2010) 405–416, https://doi.org/10.1111/j.1467-9868.2010.00746.x.
[30] S. Zhang, F. Gelain, X. Zhao, Designer self-assembling peptide nanofiber scaffolds for 3D tissue cell cultures, Semin. Cancer Biol. 15 (2005) 413–420, https://doi.org/10.1016/j.semcancer.2005.05.007.
[31] K. Seunarine, D.O. Meredith, M.O. Riehle, C.D.W. Wilkinson, N. Gadegaard, Biodegradable polymer tubes with lithographically controlled 3D micro- and nanotopography, Microelectron. Eng. 85 (2008) 1350–1354, https://doi.org/10.1016/j.mee.2008.02.002.
[32] L.M. Murray, V. Nock, J.J. Evans, M.M. Alkaisi, The use of substrate materials and topography to modify growth patterns and rates of differentiation of muscle cells, J. Biomed. Mater. Res. A 104 (2016) 1638–1645, https://doi.org/10.1002/jbm.a.35696.
[33] J.L. Lowery, N. Datta, G.C. Rutledge, Effect of fiber diameter, pore size and seeding method on growth of human dermal fibroblasts in electrospun poly(3-caprolactone) fibrous mats, Biomaterials 31 (2010) 491–504, https://doi.org/10.1016/j.biomaterials.2009.09.072.
[34] A. Timnak, J.A. Gerstenhaber, K. Dong, Y. El Har-El, P.I. Lelkes, Gradient porous fibrous scaffolds: a novel approach to improving cell penetration in electrospun scaffolds, Biomed. Mater. 13 (2018), https://doi.org/10.1088/1748-605X/aadbbe.
[35] V. Härmä, J. Virtanen, R. Mäkelä, A. Happonen, J.P. Mpindi, M. Knuuttila, P. Kohonen, J. Lötjönen, O. Kallioniemi, M. Nees, A comprehensive panel of three-dimensional models for studies of prostate cancer growth, invasion and drug responses, PLoS One 5 (2010), https://doi.org/10.1371/journal.pone.0010431.
[36] L. Chen, Z. Xiao, Y. Meng, Y. Zhao, J. Han, G. Su, B. Chen, J. Dai, The enhancement of cancer stem cell properties of MCF-7 cells in 3D collagen scaffolds for modeling of cancer and anti-cancer drugs, Biomaterials 33 (2012) 1437–1444, https://doi.org/10.1016/j.biomaterials.2011.10.056.
[37] K. Chitcholtan, E. Asselin, S. Parent, P.H. Sykes, J.J. Evans, Differences in growth properties of endometrial cancer in three dimensional (3D) culture and 2D cell monolayer, Exp. Cell Res. 319 (2013) 75–87, https://doi.org/10.1016/j.yexcr.2012.09.012.
[38] M. Zanoni, F. Piccinini, C. Arienti, A. Zamagni, S. Santi, R. Polico, A. Bevilacqua, A. Tesei, 3D tumor spheroid models for *in vitro* therapeutic screening: a systematic approach to enhance the biological relevance of data obtained, Sci. Rep. 6 (2016), https://doi.org/10.1038/srep19103.
[39] L.R. Gomes, C.R.R. Rocha, D.J. Martins, A.P.Z.P. Fiore, G.S. Kinker, A. Bruni-Cardoso, C.F.M. Menck, ATR mediates cisplatin resistance in 3D-cultured breast cancer cells via translesion DNA synthesis modulation, Cell Death Dis. 10 (2019) 459, https://doi.org/10.1038/s41419-019-1689-8.
[40] K. Rea, F. Roggiani, L. De Cecco, F. Raspagliesi, M.L. Carcangiu, J. Nair-Menon, M. Bagnoli, I. Bortolomai, D. Mezzanzanica, S. Canevari, A. Kourtidis, P.Z. Anastasiadis, A. Tomassetti, Simultaneous E-cadherin and PLEKHA7 expression negatively affects E-cadherin/EGFR mediated ovarian cancer cell growth, J. Exp. Clin. Cancer Res. 37 (2018), https://doi.org/10.1186/s13046-018-0796-1.
[41] D. Yip, C.H. Cho, A multicellular 3D heterospheroid model of liver tumor and stromal cells in collagen gel for anti-cancer drug testing, Biochem. Biophys. Res. Commun. 433 (2013) 327–332, https://doi.org/10.1016/j.bbrc.2013.03.008.
[42] Y. Imamura, T. Mukohara, Y. Shimono, Y. Funakoshi, N. Chayahara, M. Toyoda, N. Kiyota, S. Takao, S. Kono, T. Nakatsura, H. Minami, Comparison of 2D- and 3D-culture models as drug-testing platforms in breast cancer, Oncol. For. Rep. 33 (2015) 1837–1843, https://doi.org/10.3892/or.2015.3767.
[43] J. He, X. Liang, F. Luo, X. Chen, X. Xu, F. Wang, Z. Zhang, P53 is involved in a three-dimensional architecture-mediated decrease in chemosensitivity in colon cancer, J. Cancer 7 (2016) 900–909, https://doi.org/10.7150/jca.14506.
[44] B.C.K. Brunton Laurence L, Randa Hilal-Dandan, Goodman and Gilman's : the Pharmacological Basis of Therapeutics, thirteenth ed., McGraw-Hill, New York, 2018, https://doi.org/10.1017/CBO9781107415324.004.
[45] S. Xu, Z. Yang, J. Zhang, Y. Jiang, Y. Chen, H. Li, X. Liu, D. Xu, Y. Chen, Y. Yang, Y. Zhang, D. Li, J. Xia, Increased levels of β-catenin, LEF-1, and HPA-1 correlate with poor prognosis for acral melanoma with negative BRAF and NRAS mutation in BRAF exons 11 and 15 and NRAS exons 1 and 2, DNA Cell Biol. 34 (2015) 69–77, https://doi.org/10.1089/dna.2014.2590.
[46] S. Verykiou, R. Ellis, P. Lovat, Established and emerging biomarkers in cutaneous malignant melanoma, Healthcare 2 (2014) 60–73, https://doi.org/10.3390/healthcare2010060.
[47] C. Wenzel, B. Riefke, S. Gründemann, A. Krebs, S. Christian, F. Prinz, M. Osterland, S. Golfier, S. Räse, N. Ansari, M. Esner, M. Bickle, F. Pampaloni, C. Mattheyer, E.H. Stelzer, K. Parczyk, S. Prechtl, P. Steigemann, 3D high-content screening for the identification of compounds that target cells in dormant tumor spheroid regions, Exp. Cell Res. 323 (2014) 131–143, https://doi.org/10.1016/j.yexcr.2014.01.017.